Measurement of spatially nonuniform phase changes of a light beam utilizing the reflectivity characteristic of a self-pumped phase-conjugate mirror

Xiangzhao Wang
Osami Sasaki, MEMBER SPIE
Takamasa Suzuki, MEMBER SPIE
Takeo Maruyama
Niigata University
Faculty of Engineering
Niigata 950-2181
Japan

Abstract. We describe a new method for measuring spatially nonuniform phase changes of a light beam from the spatial nonuniformity of the phase changes, which is obtained by detecting the relative reflectivity change of a self-pumped phase-conjugate mirror. The method is designed to decrease the accumulation of calculating errors. The usefulness of these methods is verified through computer simulations and measurements of the phase changes caused by spatially nonuniform deformation of a semitransparent sheet of silicone gum. [S0091-3286(99)00609-1]

Subject terms: Phase change; optical testing; phase-conjugate reflectivity; optical phase conjugation; photorefractive crystal.

Paper 980155 received Apr. 17, 1998; revised manuscript received Mar. 18, 1999; accepted for publication Mar. 25, 1999.

1 Introduction

The response characteristics of a self-pumped phase-conjugate mirror (SPPCM) with respect to phase changes of the incident wave have been investigated.[1-3] When an input signal wave with a phase distribution α_0 is incident on a photorefractive crystal, an index grating corresponding to the phase distribution α_0 is formed in the crystal and a phase-conjugate wave is generated. When a spatially uniform phase change $\Delta\alpha$ occurs in the incident wave, the index grating in the crystal does not decay and the reflectivity of the SPPCM does not change. The phase change of the phase-conjugate wave is identical to the uniform phase change impressed on the incident beam. This characteristic of the SPPCM makes it possible to modulate the phase of the phase-conjugate wave by the phase modulation of the incident wave. In a laser diode (LD) interferometer with a SPPCM a phase-shifting technique can be used by modulating the uniform phase of the incident wave by varying the LD frequency, which offers improvements in measurement accuracy.[4,5] In a phase-conjugate Fizeau interferometer for surface profile measurements described in Ref. 6, spatially uniform phase changes of the incident wave caused by vibrations of object surfaces are not reversed in the phase-conjugate wave, and therefore the interferometer is insensitive to object vibrations.

When the phase of the incident wave changes in a spatially nonuniform manner, the phase change is not reversed in the phase-conjugate wave immediately after the phase change, while the reflectivity of the SPPCM decreases due to the erasing effect on the index grating. The reduction of the reflectivity is proportional to the nonuniformity of the phase change. This proportionality relation makes it possible to measure the spatial nonuniformity of phase changes of a light wave by detecting the relative reflectivity reduction of a SPPCM. In this paper the spatially nonuniform phase changes of the light wave are evaluated from the spatial nonuniformity. Because even a low spatial nonuniformity of the phase changes causes a substantial reduction of the reflectivity of the SPPCM, the measurement of the phase changes using the reflectivity characteristic of a SPPCM has a high sensitivity. In the experiments of Ref. 1 a spatial nonuniformity of 0.1 rad/mm caused the reflectivity of the SPPCM to decrease by $\approx 14\%$.

The spatially nonuniform phase change $\Delta\alpha$ of a light beam can be measured with optical interferometric methods. However, when the light beam is diffusely reflected from a rough surface or transmitted through a transparent diffuser, it is difficult to get a strong interference signal because of the annoying speckle patterns. In this situation the use of a SPPCM is effective.[7-9] If the phase change $\Delta\alpha$ is evaluated from the spatial nonuniformity of $\Delta\alpha$ obtained from reflectivity changes of a SPPCM, the effects of speckle patterns do not exist.

In Sec. 2, the method of calculating the phase change $\Delta\alpha$ from the spatial nonuniformity D is described. A method to reduce progressive calculating errors is discussed. Computer simulations are done in Sec. 3. The $\Delta\alpha$ distributions calculated along one, two, and three directions are analyzed and compared. In Sec. 4, the spatially nonuniform phase changes generated by deforming a semitransparent sheet of silicone gum are measured from the spatial nonuniformity of the phase changes, which is obtained from reflectivity changes of a SPPCM.

2 Principle

When the phase of the incident wave changes by $\Delta\alpha$ in a spatially nonuniform manner, a new incident wave is written in the crystal. In the writing process, the old index grating is erased and a new index grating corresponding to

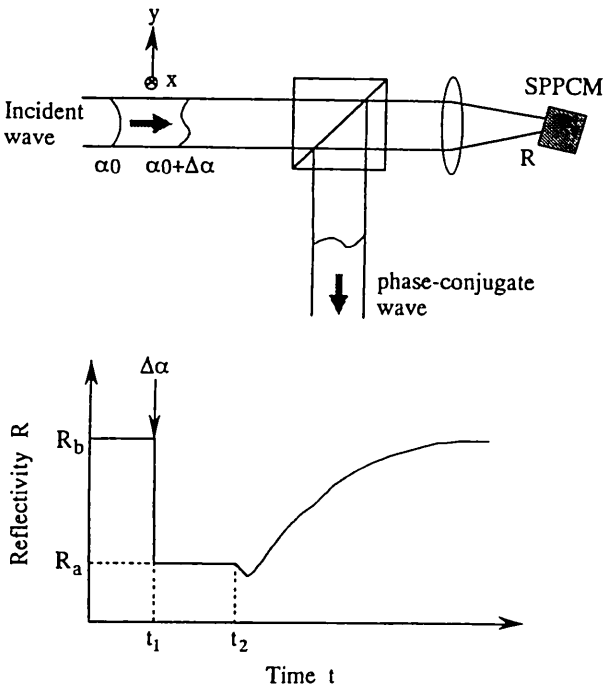

Fig. 1 Reflectivity change of a SPPCM with time before and after the phase of the incident wave changes in a spatially nonuniform manner.

the new incident wave is formed. Because of the slow response of the crystal, the old and new gratings exist in the crystal simultaneously over the decay time of the old grating. Figure 1 shows the reflectivity change of a SPPCM before and after the spatially nonuniform phase change. The phase change $\Delta\alpha$ occurs at $t=t_1$. At the same time, the reflectivity of the SPPCM decreases from R_b to R_a due to the erasure of the old index grating. Between t_1 and t_2, the old grating dominates in the SPPCM and the reflectivity R of the SPPCM scarcely changes. After $t=t_2$ the decay of the old grating quickens and R increases gradually with the formation of the new index grating.

The spatial nonuniformity D of phase change $\Delta\alpha$ of the incident beam was defined as[1]

$$D(x,y)=\left[\left(\frac{\partial\Delta\alpha}{\partial x}\right)^2+\left(\frac{\partial\Delta\alpha}{\partial y}\right)^2\right]^{1/2}. \tag{1}$$

where x and y are Cartesian coordinates on the cross section of the beam as shown in Fig. 1. The relation between the relative reflectivity reduction R_a/R_b of the SPPCM and the spatial nonuniformity D of the phase change of the incident wave has been proved experimentally to be

$$D=C\left(\frac{R_b}{R_a}-1\right), \tag{2}$$

where C is a proportionality constant. Equation (2) describes the reflectivity characteristic of a SPPCM. When the phase change of an incident wave is spatially uniform, $D=0$ and $R_a=R_b$. If the phase of the incident wave changes nonuniformly, R_b/R_a increases from 1.

When a light beam with a spatially nonuniform phase change is incident on a SPPCM, the phase change of the light beam can be measured by detecting the relative reflectivity reduction R_a/R_b of the SPPCM and using Eqs. (1) and (2).

Now, we consider how to calculate the phase changes of the light beam when the spatial nonuniformity D is known. In the discrete representation Eq. (1) can be written as

$$D(i,j)=\left[\left(\frac{\Delta\alpha(i+1,j)-\Delta\alpha(i,j)}{\Delta x}\right)^2+\left(\frac{\Delta\alpha(i,j+1)-\Delta\alpha(i,j)}{\Delta y}\right)^2\right]^{1/2}$$
$$(i=1,\ldots,N-1,\quad j=1,\ldots,N-1), \tag{3}$$

where Δx and Δy are the spatial intervals of the measurement points of $D(i,j)$ in the directions of the x and y axes, respectively, and N is the number of measurement points in the direction of the x or y axis.

In Eq. (3), $D(i,j)$ is known and there are three variables $\Delta\alpha(i,j)$, $\Delta\alpha(i,j+1)$, and $\Delta\alpha(i+1,j)$. We calculate one of them on the condition that the other two variables have been determined. To start the calculations, initial values of the other two variables are necessary. Here boundary conditions are used for the initial values. There are three methods, according to which variable is calculated:

(a) $\Delta\alpha(i,j+1)$ is calculated by the equation

$$\Delta\alpha(i,j+1)=\Delta\alpha(i,j)\pm\Delta y\left[D(i,j)^2-\left(\frac{\Delta\alpha(i+1,j)-\Delta\alpha(i,j)}{\Delta x}\right)^2\right]^{1/2}$$
$$(i=1,\ldots,N-1,\quad j=1,\ldots,N-1), \tag{4}$$

with boundary conditions $\Delta\alpha(N,j)$ and $\Delta\alpha(i,1)$ $(i,j=1,\ldots,N)$, where the upper sign is for $\Delta\alpha(i,j+1)\geq\Delta\alpha(i,j)$ and the lower sign is for $\Delta\alpha(i,j+1)<\Delta\alpha(i,j)$.

(b) $\Delta\alpha(i+1,j)$ is calculated by the equation

$$\Delta\alpha(i+1,j)=\Delta\alpha(i,j)\pm\Delta x\left[D(i,j)^2-\left(\frac{\Delta\alpha(i,j+1)-\Delta\alpha(i,j)}{\Delta y}\right)^2\right]^{1/2}$$
$$(i=1,\ldots,N-1,\quad j=1,\ldots,N-1), \tag{5}$$

with boundary conditions $\Delta\alpha(1,j)$ and $\Delta\alpha(i,N)$ $(i,j=1,\ldots,N)$, where the upper sign is for $\Delta\alpha(i+1,j)\geq\Delta\alpha(i,j)$, and the lower sign is for $\Delta\alpha(i+1,j)<\Delta\alpha(i,j)$.

(c) $\Delta\alpha(i,j)$ is calculated by the equation

$$\Delta\alpha(i,j)=\frac{\Delta y^2\Delta\alpha(i+1,j)+\Delta x^2\Delta\alpha(i,j+1)}{\Delta x^2+\Delta y^2}\pm\left[\frac{\Delta x^2\Delta y^2D(i,j)^2-\Delta y^2\Delta\alpha(i+1,j)^2-\Delta x^2\Delta\alpha(i,j+1)^2}{\Delta x^2+\Delta y^2}+\left(\frac{\Delta y^2\Delta\alpha(i+1,j)+\Delta x^2\Delta\alpha(i,j+1)}{\Delta x^2+\Delta y^2}\right)^2\right]^{1/2}$$
$$(i=N-1,\ldots,1,\quad j=N-1,\ldots,1), \tag{6}$$

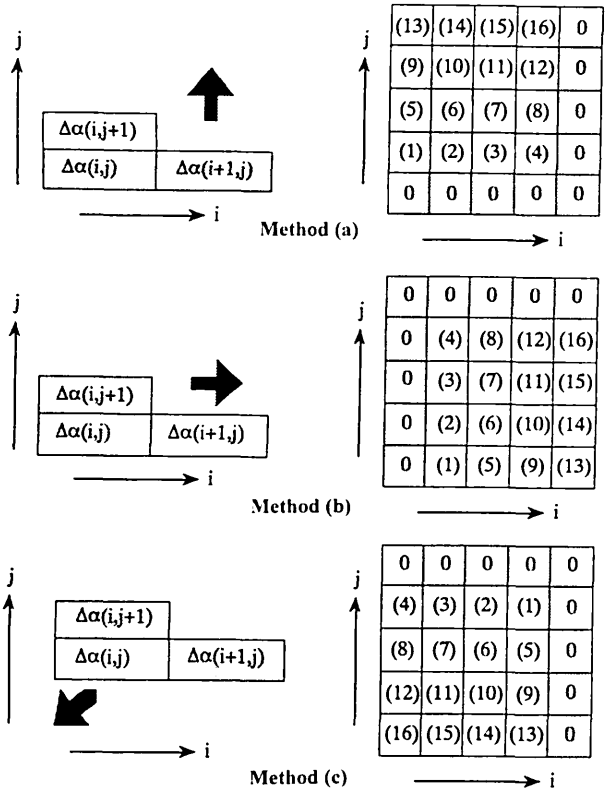

Fig. 2 Starting points and calculation directions of methods (a), (b), and (c). For simplicity, only 5×5 measurement points are considered here. The boundary conditions are zero values. The numbers in parentheses show the calculation sequences of the methods.

with boundary conditions $\Delta\alpha(N,j)$ and $\Delta\alpha(i,N)$ $(i,j=1,\ldots,N)$, where the upper sign is for $\Delta\alpha(i,j) \geq [\Delta y^2\Delta\alpha(i+1,j)+\Delta x^2\Delta\alpha(i,j+1)]/(\Delta x^2+\Delta y^2)$, and the lower sign is for $\Delta\alpha(i,j)<[\Delta y^2\Delta\alpha(i+1,j)+\Delta x^2\Delta\alpha(i,j+1)]/(\Delta x^2+\Delta y^2)$.

We illustrate the three methods in Fig. 2. First we consider method (a) of Eq. (4). The boundary conditions of Eq. (4), for simplicity, are assumed to be $\Delta\alpha(N,j)=\Delta\alpha(i,1)=0$ $(i,j=1,\ldots,N)$. Figure 2(a) shows the starting points and the calculation direction to calculate $\Delta\alpha$ using Eq. (4). The numbers in parentheses show the calculation sequence. For simplicity only 5×5 measuring points are considered here. First $\Delta\alpha(1,2)$ is calculated from the boundary conditions $\Delta\alpha(1,1)=\Delta\alpha(2,1)=0$, then $\Delta\alpha(2,2)$ from $\Delta\alpha(2,1)=\Delta\alpha(3,1)=0$, and lastly $\Delta\alpha(4,5)$ from $\Delta\alpha(4,4)=\Delta\alpha(5,4)=0$. The boundary conditions $\Delta\alpha(i,1)$ and $\Delta\alpha(i+1,1)$ are used to calculate $\Delta\alpha(i,2)$. The boundary condition $\Delta\alpha(N,j)=0$ is used to calculate $\Delta\alpha(N-1,j+1)$.

Similarly, we use Eq. (5) or Eq. (6) to calculate $\Delta\alpha$. Because of the different boundary conditions, the starting points and calculation sequences are different, as shown in Fig. 2(b) and 2(c).

It is feasible to calculate $\Delta\alpha$ using the above equations. But the shortcomings of these calculation methods are evident. Take Eq. (4) for example. Since $\Delta\alpha(i,j+1)$ is calculated from $\Delta\alpha(i,j)$ and $\Delta\alpha(i+1,j)$, and $\Delta\alpha(i,j)$ from

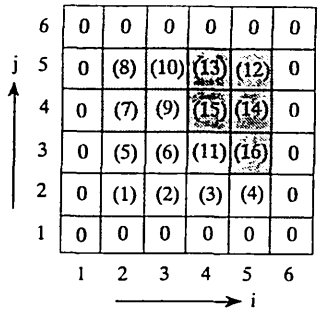

Fig. 3 Starting points and switching of calculation directions for $\Delta\alpha$.

$\Delta\alpha(i,j-1)$ and $\Delta\alpha(i+1,j-1)$, the calculating error of $\Delta\alpha(i,j-1)$ or $\Delta\alpha(i+1,j-1)$ is passed on to $\Delta\alpha(i,j+1)$. The errors are accumulated and increase with the incrementation of j.

In order to restrain the progressive errors in calculating $\Delta\alpha$, we use the three methods in turn. A value of $\Delta\alpha(i,j+1)$ is calculated by the substitution of $\Delta\alpha(i,j)$, $\Delta\alpha(i+1,j)$, and $D(i,j)$ into Eq. (4). Then substituting the values of $\Delta\alpha(i,j+1)$, $\Delta\alpha(i,j)$, and $\Delta\alpha(i+1,j)$ into Eq. (3) gives the spatial nonuniformity of $\Delta\alpha$ at the measuring point (i,j), which is denoted by $D_c(i,j)$ to distinguish it from the experimental datum $D(i,j)$. Let ϵ be a calculation tolerance. If the relation

$$|D_c(i,j)-D(i,j)|^2<\epsilon \tag{7}$$

holds, the calculation of $\Delta\alpha$ continues. When the left side of the inequality is greater than or equal to ϵ at a certain point (i,j), instead of Eq. (4), Eq. (5) or Eq. (6) is used to calculate the remaining $\Delta\alpha$ values.

Figure 3 shows an example of calculating $\Delta\alpha$ with Eqs. (4), (5), and (6). The boundary conditions for the calculations are assumed to be $\Delta\alpha(6,j)=\Delta\alpha(i,1)=\Delta\alpha(1,j)=\Delta\alpha(i,6)=0$ $(i,j=1,\ldots,6)$. The calculation sequence is indicated by the numbers in parentheses. Equation (4) is used first with the boundary conditions $\Delta\alpha(6,j)=\Delta\alpha(i,1)=0$. The inequality (7) is satisfied until the point (3, 3). At the point (4, 3), the accumulation of calculation errors results in a larger value of the left side of the inequality (7) than the calculation tolerance ϵ. Therefore, instead of Eq. (4), the calculations of $\Delta\alpha$ are continued with Eq. (5). The calculations begin from point (2, 4) with the boundary conditions $\Delta\alpha(1,j)=\Delta\alpha(i,6)=0$ $(i,j=1,\ldots,6)$. When the inequality (7) fails to hold again at point (4, 4), Eq. (5) is replaced by Eq. (6) and the remaining $\Delta\alpha$ values are calculated with the boundary conditions $\Delta\alpha(i,6)=\Delta\alpha(6,j)=0$ $(i,j=1,\ldots,6)$. Since the calculations using different equations begin with different starting points and the calculation direction changes, the progressive errors are made to decrease.

The value of ϵ in the inequality (7) has a direct bearing on the calculation errors of $\Delta\alpha$. If ϵ is so large that only one of Eqs. (4) to (6) is needed to complete the calculation of $\Delta\alpha$, relatively large progressive errors in the calculation are inevitable. On the other hand, a too small ϵ value brings the calculation to an end before completing the calculation of $\Delta\alpha(i,j)$ $(i=1,\ldots,N,\ j=1,\ldots,N)$ even if Eqs. (4) to (6) are

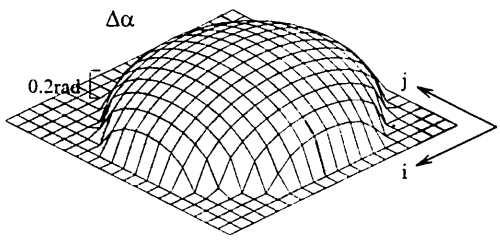

Fig. 4 A phase-distribution change used in computer simulations.

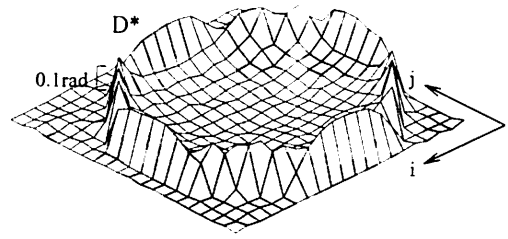

Fig. 6 Spatial nonuniformity D^* obtained by adding noise with a normal distribution to the nonuniformity D of Fig. 5. The rms value of the noise is 8% of that of D.

used in turn. We determine a minimum of the calculation tolerance ϵ with which the calculation of $\Delta\alpha$ can be completed using Eqs. (4) to (6).

The sign $\pm$ in Eqs. (4) to (6) is determined through the analysis of the distribution of spatial nonuniformity $D(i,j)$ and the comparison between ϵ values obtained for different determinations of the sign. Concrete examples are given in Secs. 3 and 4.

3 Computer Simulation

Figure 4 shows an ellipsoidal distribution of phase change $\Delta\alpha$ as described by the equation

$$\Delta\alpha(i,j)=c\left[1-\frac{(i-10)^2}{a^2}-\frac{(j-10)^2}{b^2}\right]^{1/2} \quad (i=1,...,20,\quad j=1,...,20), \tag{8}$$

where $a=9$, $b=8$, and $c=0.5$. Here 20×20 measuring points are located at unit spatial intervals in both the i-axis and j-axis directions. The boundary conditions of Eqs. (4) to (6) are $\Delta\alpha(20,j)=\Delta\alpha(i,1)=\Delta\alpha(1,j)=\Delta\alpha(i,20)=0$ $(i=1,...,20,\ j=1,...,20)$. The spatial nonuniformity D of $\Delta\alpha$ calculated from Eq. (1) is shown in Fig. 5. Since the nonuniformity $D(i,j)$ reflects the rate of $\Delta\alpha$ change at the measuring point (i,j), it has comparatively large values at the edge of the semiellipsoid in Fig. 4. With an increment of the $\Delta\alpha$ value, the D value decreases. It drops to a minimum at the vertex of the semiellipsoid $(i=10,\ j=10)$. Adding a noise to the nonuniformity D, we obtained the nonuniformity D^*, which is shown in Fig. 6. The noise consisted of random numbers with a normal distribution. The rms value of the noise was 8% of that of D. In this section, a phase distribution change $\Delta\alpha^*$ is calculated from the spatial nonuniformity D^* using Eqs. (4) to (6).

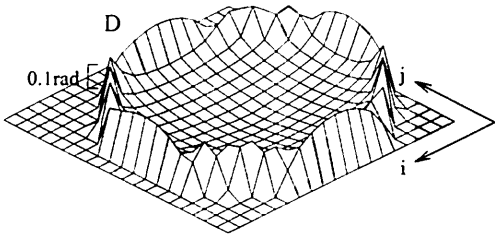

Fig. 5 Spatial nonuniformity D of the phase distribution change $\Delta\alpha$ of Fig. 4, calculated with Eq. (1).

First, with Eq. (4) a phase distribution $\Delta\alpha_1^*$ is calculated from nonuniformity D^* in the j-axis direction. Before the calculation, we consider the appropriate choice of the sign $\pm$ in Eq. (4). It is known from Fig. 4 that the sign in Eq. (4) is plus if $j<10$ and minus if $i\geq10$. The dividing line across which the sign changes from plus to minus is $j=10$. When $\Delta\alpha_1^*$ is calculated from a nonuniformity measured in experiments, the determination of the dividing line is somewhat complicated because only the nonuniformity, the boundary conditions, and a broad outline of the phase-distribution change are known. Now we determine the dividing line for the sign according to the D^* distribution in Fig. 6. It is simple to infer the dividing line from the D distribution shown in Fig. 5. It is a straight line $(j=10)$ formed by connecting the points where the $D(i,j)$ has its minimum in the j-axis direction. In the case of D^*, the dividing line cannot be determined simply by connecting the minima of $D^*(i,j)$ in the j-axis direction, owing to the effect of the noise. But it can be judged to be close to the line $j=10$. The final determination of the dividing line is made by comparing the values of the calculation tolerance ϵ at which the calculation of phase distribution changes is completed. When the dividing line was taken at $j=9$ or $j=11$, the ϵ value increased by 16% over that at the dividing line of $j=10$. Thus the dividing line was concluded to be $j=10$. Figure 7 shows the phase-distribution change $\Delta\alpha_1^*$ calculated with Eq. (4) from the D^* distribution by use of the boundary condition $\Delta\alpha_1^*(20,j)=\Delta\alpha_1^*(i,1)=0$ $(i=1,...,20,\ j=1,...,20)$.

Comparing Fig. 7 with Fig. 4, it is clear that the progressive calculation errors are relatively small initially. The er-

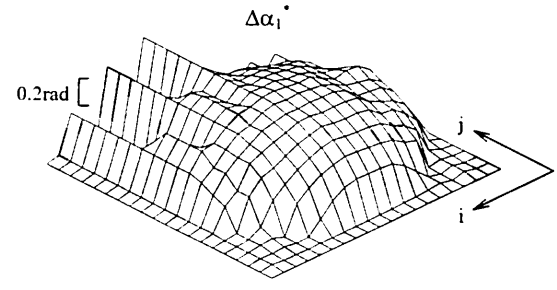

Fig. 7 Phase-distribution change calculated from the nonuniformity D^* with Eq. (4) in the j-axis direction. The dividing line for changing the $\pm$ sign in Eq. (4) from plus to minus was $j=10$.

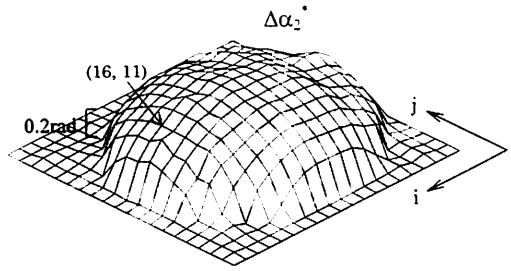

Fig. 8 Phase-distribution change calculated from the nonuniformity D^* in the directions along which j increases and decreases. Equation (4) was replaced by Eq. (6) at the measurement point (16, 11).

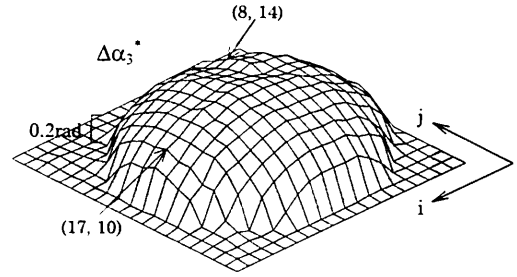

Fig. 9 Phase-distribution change calculated from the nonuniformity D^* in three different directions. Equation (5) was switched to Eq. (4) at the measuring point (8, 14), and then to Eq. (6) at the point (17, 10).

rors obviously increase with the incrementation of j. The difference between the phase-distribution changes in Figs. 4 and 7 is 34% of the rms value of $\Delta\alpha$. Next, with Eqs. (4) and (6) we calculated the phase distribution $\Delta\alpha_2^*$ from the nonuniformity D^*. Using Eq. (4) we started by calculating $\Delta\alpha_2^*$ in the direction along which j increased. The boundary condition was $\Delta\alpha_2^*(20,j)=\Delta\alpha_2^*(i,1)=0 \quad (i,j=1,...,20)$. The calculation tolerance ϵ was determined to be 6% of the rms value of D^*. The progressive error increased with the continuation of the calculation. At the measuring point (16, 11) the inequality (7) did not hold. The calculation with Eq. (4) ended at this point. The remaining $\Delta\alpha_2^*$ values were calculated using Eq. (6) in the direction along which j decreased. The boundary condition $\Delta\alpha_2^*(20,j)=\Delta\alpha_2^*(i,20)=0 \quad (i,j=1,...,20)$ was used. Figure 8 shows the calculated result. In comparison with Fig. 7, it is obvious that the progressive errors have decreased. The difference between the $\Delta\alpha_2^*$ and $\Delta\alpha$ distributions is 6.2% of the rms value of $\Delta\alpha$.

Finally, using Eqs. (4), (5), and (6), a phase-distribution change $\Delta\alpha_3^*$ was calculated from the nonuniformity D^* in the three different directions. Equation (5) was used first. In Fig. 8 the progressive errors are relatively large near the boundary line $i=1$. The errors near that boundary line were decreased by using Eq. (5) with the boundary condition $\Delta\alpha_3^*(1,j)=\Delta\alpha_3^*(i,20)=0 \quad (i,j=1,...,20)$ and calculating $\Delta\alpha_3^*$ in the direction along which i increased. Hence the calculating tolerance ϵ was chosen to be 5% of the rms value of D^*. Equation (5) was switched to Eq. (4) at the measuring point (8, 14). After that, Eq. (4) was switched to Eq. (6) at the point (17, 10). Figure 9 shows the calculated $\Delta\alpha_3^*$ distribution. The difference between $\Delta\alpha_3^*$ and $\Delta\alpha$ is 5% of the rms value of $\Delta\alpha$. Compared with the $\Delta\alpha_2^*$ distribution, it is found that the rising part in the i-axis direction has been improved.

4 Experiments

Figure 10 shows an experimental setup to detect spatial nonuniformity of phase changes of an incident wave. The light beam from a single-mode argon-ion laser at $\lambda=514.5\,\text{nm}$ was expanded with a microscopic objective lens L_1 and lens L_2 into a 35-mm-diam beam. A sheet of 0.5-mm-thick semitransparent silicone gum was placed between the lens L_2 and the beam splitter BS. Three sides of the sheet silicone gum was fixed as shown in the lower figure. The beam transmitted through the gum sheet was focused with a lens L_3 into a SPPCM of $BaTiO_3$ crystal. The phase-conjugate wave from the SPPCM was directed by the beamsplitter BS to a plane C. The plane C was taken so that the distance between it and the $BaTiO_3$ crystal was equal to that between the gum sheet and the crystal. The light field of the phase-conjugate wave on C was imaged on a 2-D CCD image sensor by a lens L_4. The 20×20 photodetector elements in the CCD image sensor were used to detect the intensity distribution of the light field. The intervals of the measured points were 1.0 mm. The measured region was 20 mm×20 mm.

First, a steady-state intensity distribution of the phase-conjugate wave was detected; then the gum sheet was given a spatially nonuniform deformation by touching it lightly at a point. The deformation of the sheet caused a spatially nonuniform phase-distribution change of the beam incident on the $BaTiO_3$ crystal. That change resulted in a decrease of the phase-conjugate reflectivity of the crystal immedi-

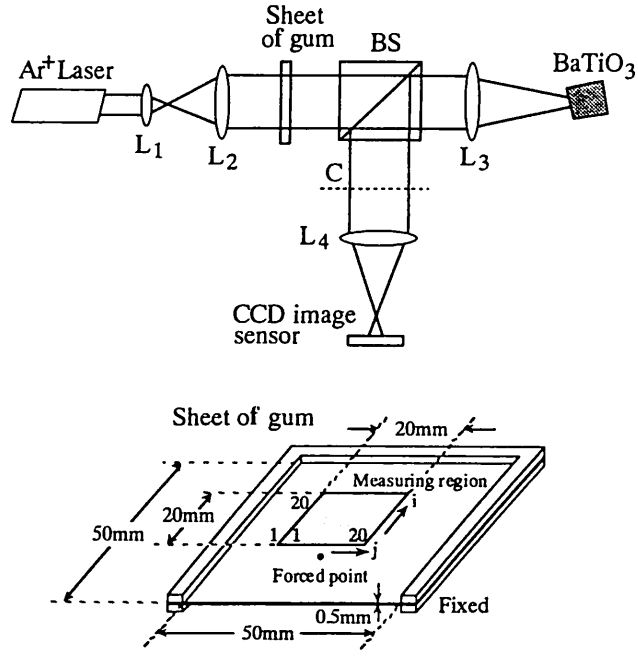

Fig. 10 Experimental setup for detecting spatial nonuniformity of the phase changes of incident wave that are caused by deformation of a semitransparent gum sheet.

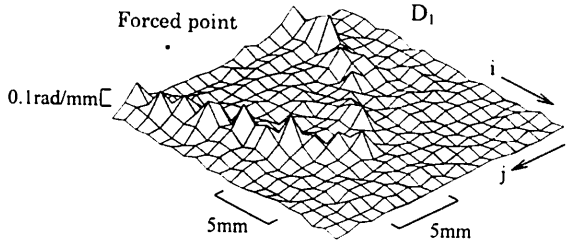

Fig. 11 Spatial nonuniformity D_1 of the phase-distribution change of the incident wave caused by deformation of the sheet of silicone gum. It was obtained by substituting the relative reflectivity reduction of the SPPCM into Eq. (2).

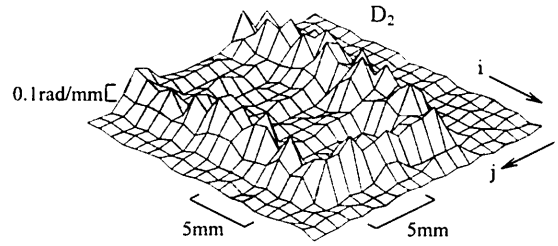

Fig. 13 Spatial nonuniformity D_2 of the phase-distribution change of the incident wave obtained after augmenting the deformation of the gum sheet.

ately after the sheet was touched. The intensity distribution of the phase-conjugate wave was detected, and the relative reduction of the phase-conjugate reflectivity of the crystal was calculated from the intensity values of the phase-conjugate wave detected before and after touching the sheet. The spatial nonuniformity D of the phase changes of incident wave was obtained by substituting the relative reflectivity reduction into Eq. (2). The proportionality constant C in Eq. (2) was chosen to be 0.6 rad/mm.[1]

Figure 11 shows the obtained spatial nonuniformity, which is denoted by D_1. The D_1 values at the three boundary lines of the measured region other than $i=1$ are very small. Their average value is less than 10% of the maximum of D_1. Since the two sides of the gum sheet along the i axis and one side near the line $i=20$ along the j axis were fixed, we deduced that the phases of the incident wave transmitted through the boundaries at $i=20$, $j=1$, and $j=20$ did not change. Thus we had the boundary conditions $\Delta\alpha(i,1)=\Delta\alpha(i,20)=\Delta\alpha(20,j)=0$ $(i,j=1,\ldots,20)$, which were used for Eqs. (4) and (6). It was found from Fig. 11 that the D_1 distribution was approximately symmetrical about the line $j=12$. The phase-distribution change $\Delta\alpha_1$ of the incident wave was calculated with Eq. (4) on the condition that $j=12$ was the dividing line. It was also calculated assuming that the dividing line was $j=11$ and $j=13$. In comparison with the case of $j=12$, the calculating tolerance ϵ needed to complete the $\Delta\alpha_1$ calculation increased by 180% and 90% in the cases of $j=11$ and $j=13$, respectively. Thus the dividing line was determined to be $j=12$. After that, the phase-distribution change $\Delta\alpha_1$ was calculated again with Eqs. (4) and (6). The calculating tolerance ϵ was chosen to be 7.2% of the rms value of D_1. Equation (4) was switched to Eq. (6) at the measurement point (13, 11). Figure 12 shows the calculated result. The middle part of the $\Delta\alpha_1$ distribution arches. Its maximum is 0.465 rad.

On augmenting the deformation of the gum sheet, a spatial nonuniformtiy D_2 of phase changes of the incident wave was obtained, which is shown in Fig. 13. The augmentation of deformation resulted in an increment in spatial nonuniformity. From the D_2 distribution the phase-distribution change $\Delta\alpha_2$ of the incident wave was calculated with Eqs. (4) and (6). In the same way as previously, the dividing line in the j-axis direction was determined to be $j=12$. The calculating tolerance ϵ was 11.4% of the rms value of D_2. Equation (4) was replaced by Eq. (6) at the measurement point (4, 11). Figure 14 shows the calculated $\Delta\alpha_2$ distribution. Its maximum is 0.884 rad.

5 Conclusion

We have proposed a new method for measuring spatially nonuniform phase changes of a light beam. The changes were calculated from the spatial nonuniformity of the phase changes obtained by detecting the reflectivity changes of a SPPCM. The computer simulations made it clear that the progressive calculating errors of the phase changes were decreased by the change in calculation directions and the use of different boundary conditions. In the experiments, we obtained spatial nonuniformity of phase changes generated by deforming a semitransparent sheet of silicone gum, and calculated the spatially nonuniform phase changes caused by the deformation. The results show the feasibility of the new measurement method for spatially nonuniform phase changes.

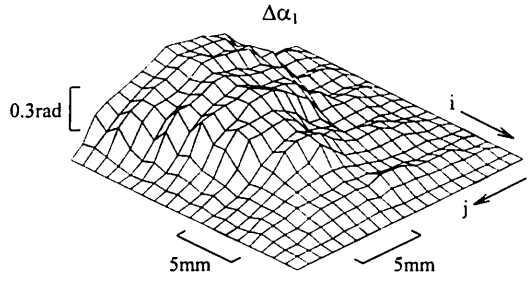

Fig. 12 Phase-distribution change $\Delta\alpha_1$ of the incident wave calculated from the nonuniformity D_1 of Fig. 11.

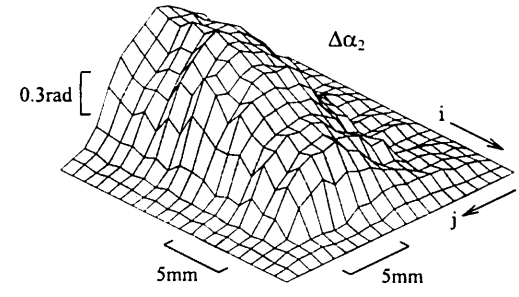

Fig. 14 Phase-distribution change $\Delta\alpha_2$ of the incident wave calculated from the nonuniformity D_2 of Fig. 13.

References

1. X. Wang, O. Sasaki, T. Suzuki, and T. Maruyama, "Response characteristics of a self-pumped phase-conjugate mirror to spatially nonuniform phase changes of an incident wave and their applications," *Opt. Eng.* **34**, 1184–1190 (1995).
2. J. Feinberg, "Interferometer with a self-pumped phase-conjugating mirror," *Opt. Lett.* **8**, 569–571 (1983).
3. Y. Tomita, R. Yahalom, and A. Yariv, "Phase shift and cross talk of a self-pumped phase-conjugate mirror," *Opt. Commun.* **73**, 413–418 (1989).
4. Y. Ishii and I. Uehira, "Laser-diode phase-shifting interferometry with a self-pumped phase-conjugate mirror," *Opt. Lett.* **18**, 1459–1461 (1993).
5. T. Suzuki, J. Hasegawa, O. Sasaki, and T. Maruyama, "Sinusoidal phase-modulating laser-diode interferometer using a self-pumped phase-conjugate mirror," *Proc. SPIE* **2576**, 299–307 (1995).
6. X. Wang, O. Sasaki, Y. Takebayashi, T. Suzuki, and T. Maruyama, "Sinusoidal phase-modulating Fizeau interferometer using a self-pumped phase conjugator for surface profile measurements," *Opt. Eng.* **33**, 2670–2674 (1994).
7. M. Paul, B. Betz, and W. Arnold, "Interferometric detection of ultrasound at rough surfaces using optical phase conjugation," *Appl. Phys. Lett.* **50**, 1569–1571 (1987).
8. O. Sasaki, T. Manabe, X. Wang, and T. Suzuki, "Double sinusoidal phase-modulating laser-diode interferometer using self-pumped phase-conjugate wave for measuring displacements of rough surfaces," in PR'97 Proc., pp. 523–526 (1997).
9. X. Wang, O. Sasaki, T. Kikuchi, N. Ito, T. Suzuki, and T. Maruyama, "Vibration amplitude measurement for rough surface with an interferometer using phase-conjugate laser light," in PR'97 Proc., pp. 208–211 (1997).

Xiangzhao Wang received the BE degree in electrical engineering from Dalian University of Science and Technology, China, in 1982, and the ME and DrEng degrees in electrical engineering from Niigata University in 1992 and 1995, respectively. While this work was performed he was an assistant professor in the Department of Electrical and Electronic Engineering at Niigata University. Now he works as a professor at the Shanghai Institute of Optics and Fine Mechanics, Academia Sinica, China. His research interests include optical measuring systems, applications of phase-conjugate optics, and optical information processing.

Osami Sasaki received the BE and ME degrees in electrical engineering from Niigata University in 1972 and 1974, respectively, and the DrEng degree in electrical engineering from Tokyo Institute of Technology in 1981. He is a professor of electrical engineering at Niigata University, and since 1974 he has worked in the field of optical measuring systems and optical information processing.

Takamasa Suzuki received the BE degree in electrical engineering from Niigata University in 1982, the ME degree in electrical engineering from Touhoku University in 1984, and the DrEng degree in electrical engineering from Tokyo Institute of Technology in 1994. He is an associate professor in the Department of Electrical and Electronic Engineering at Niigata University. Since 1987 he has worked on interferometers using laser diodes and applications of phase-conjugate optics at Niigata University.

Takeo Maruyama received the BE degree in electrical engineering from Niigata University in 1965 and the DrEng degree in electrical engineering from Nagoya University in 1979. He is a professor of electrical and electronic engineering at Niigata University, and since 1965 he has worked in the field of the physics of ionized gasses and optical metrology.